

3D STRESS ESTIMATION USING ADAPTED FINITE ELEMENT MODEL
UPDATING TECHNIQUES

by

Affan Danish Khan
A Thesis
Submitted to the
Graduate Faculty
of
George Mason University
in Partial Fulfillment of
The Requirements for the Degree
of
Master of Science
Civil, Environmental, and Infrastructure Engineering

Committee:

_____	Dr. David Lattanzi, Thesis Director
_____	Dr. Girum Urgessa, Committee Member
_____	Dr. Anthony Battistini, Committee Member
_____	Dr. Liza Durant, Department Chair
_____	Dr. Kenneth S. Ball, Dean, Volgenau School of Engineering
Date: _____	Fall Semester 2016 George Mason University Fairfax, VA

3D Stress Estimation Using Adapted Finite Element Model Updating Techniques

A Thesis submitted in partial fulfillment of the requirements for the degree of Master of Science at George Mason University

by

Affan Danish Khan
Bachelor of Engineering
NED University of Engineering & Technology, 2013

Director: Dr. David Lattanzi, Assistant Professor
Department of Civil, Environmental, and Infrastructure Engineering

Fall Semester 2016
George Mason University
Fairfax, VA



This work is licensed under a [creative commons attribution-noncommercial 3.0 unported license](https://creativecommons.org/licenses/by-nc/3.0/).

DEDICATION

This is dedicated to my loving parents and my uncle and aunt for their support throughout this challenging period.

ACKNOWLEDGEMENTS

First and foremost, I am thankful to Allah Subhanahu wa Ta'ala for the countless blessings.

I would like to thank Professor Lattanzi for providing me this opportunity, and for his mentorship throughout. I am thankful to the committee members, Professor Battistini and Professor Urgessa, for their expert advice and encouragement. I am thankful to Kasra Ghahremani and Bahman Jafari for allowing me to further their research. In addition, Ali Khaloo and Jeff Bynum for their valued technical support.

I am grateful to my uncle, aunt and grandmother for their care and support at home. I would like to thank my fiancée. I am thankful to my parents and siblings without whom none of this would have been possible.

TABLE OF CONTENTS

	Page
List of Tables	vii
List of Figures	viii
List of Abbreviations	ix
Abstract	x
Chapter 1: Introduction	1
State of Practice	2
Research Need	3
Finite Element Model Updating Approach	5
Focus	5
Thesis Overview	6
Chapter 2.....	6
Chapter 3.....	7
Chapter 4.....	7
Chapter 5.....	7
Chapter 6.....	7
Chapter 2: Literature Review	8
Corrosion and Capacity Assessment	8
Terrestrial Laser Scanning (TLS)	10
Photogrammetry	12
Post-Processing	13
Summary and Research Need	14
Focus of this Thesis	14
Chapter 3: Section Loss Sensitivity Study	16
Ghahremani et al.'s Research	16
Goal of this Study	17
Methodology	19

Analysis	24
Results	27
Noise Analysis.....	32
Chapter 4: Deflection Study.....	35
Jafari et al.'s Research.....	35
Goal of this Study.....	36
Methodology & Analysis	36
Results	38
Chapter 5: Challenges & Limitations.....	40
Chapter 6: Conclusion.....	44
Future Work	45
References	48

LIST OF TABLES

Table	Page
Table 1: Observed maximum stresses and stresses below damaged hole surface, and their percentage difference	28
Table 2: Stress concentration factor comparison	31
Table 3: Stresses observed from analysis of 10 specimens	33
Table 4: Stress concentration factor comparison for 10 specimens	34
Table 5: Measured deflections and applied load (Jafari et al.)	37
Table 6: Max stresses observed for specimens	39

LIST OF FIGURES

Figure	Page
Figure 1: Ghahremani et al.'s proposed model updating approach for finite element analysis.....	18
Figure 2: Face view of point cloud for 1.5" diameter hole with 25% image noise	20
Figure 3: Side view of 1.5" diameter hole with 25% noise	20
Figure 4: (a) Imported point cloud (left) and (b) associated wire mesh (right) in MeshLab	22
Figure 5: (a) Solid model of damage (left) and (b) plate specimen updated by subtracting the damage	23
Figure 6: 1.5" diameter holes with various levels of noise	24
Figure 7: Tensile test model schematic	25
Figure 8: Ready-to-analyze section loss specimen in Autodesk Inventor	25
Figure 9: Von Mises stress profile of 1.0" diameter hole specimen with 25% noise	26
Figure 10: Key locations for stress estimation	27
Figure 11: Sharp edges and pointed locations after subtraction	29
Figure 12: Line graph of max stresses observed.....	30
Figure 13: Diagram of axial specimen for stress concentration factor calculations	31
Figure 14: FEA model for deflection study	37
Figure 15: General stress profile results: (a) due to induced load (top) and (b) due to applied point load (bottom)	38
Figure 16: Holes of sizes 1.5" and 0.5" with 25% noise	41
Figure 17: Holes meshed using octree depths of 5, 6 and 8 (from left to right)	42

LIST OF ABBREVIATIONS

American Road and Transportation Builders Association.....	ARTBA
National Bridge Inspection Standards.....	NBIS
Occupational Safety and Health Administration	OSHA
Light Detection and Ranging	LiDAR
Finite Element Analysis	FEA
Finite Element Modeling	FEM
National Association of Corrosion Engineers.....	NACE
Michigan Department of Transport.....	MDoT
American Institute of Steel Construction.....	AISC
Terrestrial Laser Scanning	TLS
Linear Variable Differential Transformer	LVDT
Electric Strain Gauge	ESG
Point Cloud	PC
Dense Structure from Motion	DSfM

ABSTRACT

3D STRESS ESTIMATION USING ADAPTED FINITE ELEMENT MODEL UPDATING TECHNIQUES

Affan Danish Khan, M.S.

George Mason University, 2016

Thesis Director: Dr. David Lattanzi

According to a 2016 study by the American Road and Transportation Builders Association (ARTBA) one bridge in every ten is structurally deficient. Two major contributors of structural deficiency are corrosion, which causes material loss and thinning of cross sections, and permanent plastic deformations. Currently, there are no standard methods for understanding how measurements of these damages impact stress and capacity analysis. The research presented in this thesis focuses on the use of 3D images to create “point clouds” for such structural capacity analysis. Using a set of previously developed techniques that measure both section loss and deformations in point clouds, two studies were performed to analyze the effectiveness of using these techniques to update corresponding finite element models. The first study was a sensitivity analysis to quantify the effect of image noise on stress concentration estimates, and to better understand the limits of the updating approach. In the second study, point cloud

deflection measurements from three-point bending tests were used to induce translations and stresses in a finite element model. The results of the first study showed that increasing image noise resulted in a higher likelihood that artifacts would form in the finite element model, leading to a localized increase in stress; however, it was also found that subsurface stresses matched the values expected from elastic theory and methods of analyzing the data with these anomalies are discussed. The findings of the second study showed that applying localized displacements in the 3D finite element model created localized stress concentrations that do not represent the expected stress profiles. While both studies provide important insight into this relatively new technology, future work to be performed might include creating methods to better differentiate between artificial stress anomalies and actual states of stress, as well as experimental validation.

CHAPTER 1: INTRODUCTION

According to a 2016 study by the American Road and Transportation Builders Association (ARTBA), of bridges with a minimum daily crossing volume of 204 million vehicles, one bridge in every ten is structurally deficient. 85% of the most travelled bridges across the country were built before 1970 and are struggling against ageing, fatigue, increased loads, obsolescence of design and weathering. The ARTBA report declared a backlog of \$115 billion in bridge work in 2015 (Jansen). As a result, federal and state departments of transportation are continuously looking at cost effective alternatives for inspection and assessment that can be implemented immediately.

Two of the major contributors of structural deficiency are corrosion and plastic deformation. Corrosion, which can be defined as electrochemical oxidation of structural steel, slowly deteriorates bridge elements, causing localized material loss, generalized thinning of the cross section, and in some instances complete section loss. Reduction of the member cross section will reduce its design capacity and can create stress concentrations. Both of these effects, as well as the trend of increasing allowable truck loads, may ultimately lead to overloading of the structure which in turn can cause permanent deformations and out of plane warping. These plastic deformations further decrease the load carrying capacity of the structure and reduce serviceability.

State of Practice

According to the Bridge Inspector's Reference Manual released in 2012 by the National Bridge Inspection Standards (NBIS), there are three basic methods for the inspection of a steel bridge member: Visual, Physical and Advanced. The manual further indicates that for each bridge, one, two or all three methods together may be required. Visual inspection is required to identify damages and their locations. Physical inspection involves using physical techniques to understand the extent and severity of the deficiencies. In the case of section loss, a straight edge and tape measure may be used to document the dimensions of the member in order to quantify section loss. Sometimes calipers or ultrasonic thickness gauges are used for exact measurements of the remaining section. Advanced inspection methods require the use of more sophisticated equipment, often by a trained technician, to gain complete understanding of visually observed damage. In the case of section loss resulting from corrosion, the use of corrosion sensors to indicate the degree of corrosion of a member may be appropriate. Other advanced tools are used mainly to detect surface and subsurface flaws and fatigue cracking (Hartle and Administration).

In all methods, the recorded measurements are used to make section loss estimates at specific point locations without considering the effect on member behavior or global structural behavior, thereby preventing accurate full field 2D or 3D stress analysis. In addition, stress concentration effects at cracks and sharp edges are ignored in the process. Furthermore, there is a lack of any quantitative or consistent use of these measurements since there are no standardized procedures for capacity analysis. Based on section loss measurements mostly, individual structural elements are categorically rated

based on qualitative analysis without analytical evaluation, thus necessitating the investigation of a means by which inspection data could be easily translated into computational model of the structure.

Visual and physical inspection requires manpower dependent on the size of the bridge under inspection and the allotted time period. It further requires employment of comprehensive safety measures within the guidelines of the Occupational Safety and Health Administration (OSHA) and training for the inspection crew is mandatory as various procedures have proven to be dangerous to inspectors. Temporary holds on traffic and closing down lanes also has direct economic impacts on the local economy. Current techniques still require visual or physical inspection of some degree, which apart from being expensive, incorporate human error. Previous studies propose the estimation of the remaining life from the design plans and drawings, which are not an accurate representation of the as-built reality and do not account for time dependent deformations and damage. Moreover, in cases of bridges over 50 years old, the original design practices employed have become obsolete and may not be well documented.

Research Need

There is a critical need to reduce the time and manpower needed for the process of bridge inspection, and to provide more quantitative capacity estimates. 3D imaging and scanning techniques are used for surveying and mapping in various fields of engineering and science and have the potential to be used in bridge inspections. A major goal of this research is to develop an analytical method to accurately capture the in situ dimensions of bridge components and translate them into a computational model that can

be used to evaluate the 3D state of stress on various components. This will provide a new method for the inspection and capacity analysis of bridges while limiting costs and inspection time.

Light Detection and Ranging (LiDAR) was initially a surveying technology that uses the principle of measuring the time it takes for a laser to travel to a subject and back, and uses that to calculate the linear distance to the subject. By sweeping multiple lasers across a subject, the LiDAR unit can define the surface of the subject in 3D using a cluster of points based on the measured distances. The result is a 3D point cloud of a subject's surface. LiDAR imaging devices are commonly known as terrestrial laser scanners (TLS) or 3D scanners.

Photogrammetry is an imaging technique based on Dense Structure from Motion (DSfM). The idea is that when moving through the space around a subject, the different angles observed allow for a 3D perception of the subject. The technique uses multiple images of a subject taken from various angles. Certain key points, like corners and apex, are found and matched across the images to align the subject. Using the matched key points and epipolar geometry, a 3D point based outline of the subject is created. This is called a sparse cloud. A dense reconstruction algorithm is then used to fill in these outlines, resulting in a dense 3D point cloud of the subject's surface, similar to those generated by LiDAR (Hartley and Zisserman).

For both LiDAR and DSfM, 3D imaging results in large data sets that are difficult to use and do not provide any inherent quantitative estimates on their own. Typically, these point clouds are meshed together to form a 3D surface which is then converted into

solid bodies compatible with finite element software packages. However, the meshing algorithms lead to smoothing of local damage that can cause a loss of critical stress information.

Finite Element Model Updating Approach

As alternatives to the typical methodology of meshing and modeling, two point cloud measurement methodologies have recently been developed, one for section loss and one for deflections (Ghahremani, Lattanzi, and Khaloo; Jafari, Khaloo, and Lattanzi). In both cases the aim is to measure and model just the damages instead of the whole specimen, and use these localized measurements to update the initial undamaged model. The damages are identified and isolated by comparing the two point clouds, an as-built and an in-situ cloud.

Deflection can be directly measured from these point clouds using open source tools or software, a technique developed and under further research (Jafari, Khaloo, and Lattanzi). In a separate study, Ghahremani et al. has proposed the meshing and modeling of the isolated section loss damages, followed by its subtraction from the original model. The isolation immensely decreases the number of points which are to be meshed and modeled, thereby reducing errors related to smoothing of local damages and improving scalability (Ghahremani, Lattanzi, and Khaloo).

Focus

The two modeling approaches are yet to be tested and explored in accordance with finite element stress analysis. The purpose of this study was to prototype the FEA model updating approach proposed by Ghahremani et al. & Jafari et al. Their techniques

were used for the first time for 3D stress estimation, to understand the challenges and limitations they pose. Two separate methodologies were studied. To expand understanding of the model updating approach for section loss by Ghahremani et al. (Ghahremani, Lattanzi, and Khaloo), and its use in static stress analysis, a sensitivity study was performed. The aim was to quantify the effects of image noise on stress concentration estimates. Image noise is referred to as the inevitable discrepancy in the point cloud that arises during the process of model generation, a problem for both LiDAR and DSfM. A plate with a hole was modeled and analyzed under axial tension. The hole was synthetically created to represent section loss. Random noise of various degrees was artificially added to the point cloud to signify image noise. The model was then analyzed in an FEA package. A deflection study was also performed on the measurements extracted from the three-point bending test of aluminum bars in Jafari et al. (Jafari, Khaloo, and Lattanzi), where the recorded deflections were used to induce translations to a FE model of the bars. The resulting bending stress profile was studied and conclusions were formed.

Thesis Overview

Chapter 2

This chapter reviews related work, including an overview of the field of 3D imaging and measurement techniques. There is a lack of research in the use of these procedures to document corrosion degradation and section loss. Hence, the literature studied pertains to the state of the art in generating point cloud data from

photogrammetry and laser scanning in other domains of structural engineering, as well as the post-processing involved.

Chapter 3

This chapter presents the experimental methodologies designed for the section loss study and subsequent analysis. This is followed by the results and findings with further discussion and analysis.

Chapter 4

This chapter presents the experimental methodologies designed for the deflection study and the analysis, followed by the declaration of the results and their explanations.

Chapter 5

This chapter explores the challenges faced and the limitations of the two studies.

Chapter 6

This chapter concludes the research findings and provides recommendations for future research on the topic.

CHAPTER 2: LITERATURE REVIEW

Corrosion and Capacity Assessment

According to the National Association of Corrosion Engineers (NACE)

International almost one-third of all the bridges in the United States are made of steel, and demand regular inspection and maintenance to check for corrosion (NACE). The electrochemical oxidation of steel can lead to section loss and thereby, a reduction in the load carrying capacity and a decrease in the remaining life of the structure. Kayser and Nowak developed deterioration models to study the effects of corrosion and record the structure's performance (Kayser and Nowak). They mentioned in their study the three effects of corrosion on structural steel: loss of material, change in section properties and accumulation of degraded metal. The research found that the webs at the ends of the beam, resisting shear forces, are the most vulnerable location for corrosion. Material and section loss in the web near supports lead to reduction in shear capacity of the girder until it fails by local buckling. Bearing capacity is equally affected by the section loss and follows a similar pattern in reduction particularly in the absence of stiffeners.

In 2006, researchers performed a durability evaluation study on both corroded specimens from the field and artificially degraded beams (Sugimoto, Kobayashi, and Ichikawa). The results were then reproduced in a non-linear FEM analysis; the purpose of which was to compare and relate the buckling phenomenon observed under bending and shear tests performed on the specimens. The static non-linear stress evaluation was

completed in ABAQUS. Recognizing how tedious it is to go in the field and accurately measure corrosion damage on each girder, this study successfully provided a strength evaluation model to estimate remaining strength based on multiple factors and the estimated measurements of the corroded regions.

In 2005, the Michigan Department of Transportation (MDOT) conducted a study to provide a quick and accurate method for determining reduced capacity of corroded steel beam bridges (van de Lindt and Ahlborn). Typical rolled beams were modelled and analyzed using commercially available finite element packages; the results were validated against laboratory experiments. The study focused on the buckling capacity of these rolled beams to develop design charts that would provide estimates of the remaining capacity of the beams within AISC code limitations. A deterioration factor can be identified from the charts after measuring and correlating the corroded heights and depth of the material. This factor when multiplied with the original design capacity, provides the remaining capacity of the steel girder.

In a 2010 study, the authors compiled thickness loss data from four corroded I-beams that were analyzed in two different methods (Sharifi and Rahgozar). The test yielded identical results which were used to develop a quantitative relation between loss of thickness and remaining moment capacity as compared to the original design capacity of a new beam. The study showed that either of the two tests can be used to obtain minimum curves for the estimation of the remaining moment capacity. However, a visual inspection and thickness measurement is still required for an accurate estimate.

Another means of predicting corrosion damage and estimating remaining useful life is by creating time dependent reliability profiles. The study by Czarnecki and Nowak focuses on creating these profiles based on a reliability analysis of the girders individually and of the structural system of the bridge as a whole, and accommodates different load models and deterioration due to corrosion (Czarnecki and Nowak).

These studies and other research on the subject of corrosion and capacity loss provide means of accurately estimating the remaining capacity of a structural steel member. However, most of these methods require tedious hands-on field work to estimate thickness or material loss or to measure dimensions of the section loss. Moreover, the process is time- and cost- consuming and requires blocking traffic for the inspection which itself is dangerous.

Terrestrial Laser Scanning (TLS)

The use of Terrestrial Laser Scanners (TLS), also known as LiDAR, for structural assessments is well documented over the past decade. The technique is to construct solid finite element models from the point cloud data extracted from laser scanning the environment. This methodology has been employed in structural engineering particularly to gather data from places otherwise difficult to access, such as roof beams (Cabaleiro et al.) and bridge girders (Conde-Carnero et al.; Guldur, Yan, and Hajjar); and to capture measurements of historical buildings (Barbieri et al.) and monuments (Zvietcovich, Castaneda, and Perucchio) that require minimal contact.

A 2015 study investigated the scenario of hanging new facilities from existing beams (Cabaleiro et al.). Original design drawings do not reflect the as-built reality of

construction nor do they account for the elastic structural deformations due to load over time. The need to acquire new data for dimensional drawings and structural calculations arises, which is a tedious, time and cost consuming process with an increased probability of errors. A LiDAR process was designed to capture this as-built state. The accuracy of the developed process depended on a number of factors including, but not limited to, distance from target, angle of incidence, and reflective properties of the surface. An algorithm to measure beam deflections by fitting a polynomial along the surface of the flange was used to model the beams, and beams within the allowed deflection limits were further modelled and analyzed to assess their ability to carry additional loads.

In stress estimation research by Lee and Park, a lab test of a beam under concentrated load at the center was monitored by linear variable displacement transducers and electrical strain gauges in addition to being laser scanned, for 3 experiments (Lee and Park). A comparison between linear variable differential transformer (LVDT) results of deflection and a n^{th} order polynomial equation applied to the 3D data corresponded to an error of less than 3%. For first two cases, the stresses estimated by the models were close to that of the electric strain gauges (ESG), with about 10MPa error. However, in the third case stress estimations were further from the expected results. This was because the flexibility matrix used to estimate the applied loads from the given deflections was more sensitive to the discretization of the beam and the error caused by the flexibility matrix increases.

A historical building underwent seismic assessment in 2012 (Barbieri et al.). Restoration aimed to redesign the existing structure according to present standards which

in this case involved the identification of the structural deficiencies and evaluation of the new load bearing capacity. To do this the structure of the building including the façade was laser scanned into a 3D model. The model was deemed accurate enough to continue with the seismic evaluation. Advanced numerical tools to perform nonlinear 3D dynamic analyses were used to investigate all possible failure mechanisms, local and global, when subjected to an earthquake. As a compromise between the conflicting requirements of reasonable computing time and accuracy of the solution, a finite element discretization based on four node tetrahedral elements was adopted depending upon the location of those elements in the structure. The key locations where the main failure mechanisms were located were discretized with elements of smaller size.

Photogrammetry

TLS or LiDAR is an expensive technology. Photogrammetry is a parallel technology that can produce similar density point clouds, the accuracy and cost of which are directly dependent on the camera and the lens. To define an appropriate structural geometry measured directly from camera pictures avoiding physical contact is known as “close range” photogrammetry. The technique employed is DSfM. Currently, there is a lack of research conducted using this technology to accommodate structural engineering applications, which is one of the primary motivations for the studies performed in this thesis.

In a 2009 paper, Armesto et al. conducted FEA using close range photogrammetry. An accurate 3D model of a girder truss including its irregularities such as damaged cross-sections and out of plane deformations was achieved, based on which a

3D FEM was created and analyzed in the software package, MSC Marc. The geometry used to build the FEM was measured under the existing loads. Convergence analyses showed that simpler meshes did not properly reflect the complex geometry and denser meshes were more appropriate for accurate numerical analysis. Dynamic analyses were performed and the result pointed out several differences between 2D and 3D models. However, only higher eigen frequencies revealed these differences. The acceptable range of discrepancies with respect to the computational cost of the analysis is an open question. Some hidden geometries of the structure had to be artificially completed (Armesto et al.). The success of this research provides evidence for future use of photogrammetry for stress analysis.

Post-Processing

The point cloud data extracted from either 3D imaging technology, TLS or photogrammetry, must be meshed and reconstructed into a solid surface and volume model.

A 2011 study presented an in-depth discussion about processing point clouds from LiDAR using industrial grade software that directly and automatically employs solid modeling, optimizes meshing and then delivers ready-to-analyze finite element models; such as KUBIT, Geomagic and others (F Laefer, Truong-Hong, and Fitzgerald). The study documents the surface reconstruction algorithms behind the various software and their limitations. The results produced made it clear that automatic 3D modeling even for rectilinear structures is rarely possible without some manual interference to achieve higher accuracy and prevent loss of data.

On the same topic, another study showed the need for post processing of the point cloud data and its automatic conversion to solid 3D models that can be discretized and analyzed (Conde-Carnero et al.). To perform this data processing, the study used commercially available 3D modeling software, Solidworks, for solid modeling and the FEA packages, ABAQUS and SAP2000, for dynamic modal and static nonlinear analyses. The purpose of the study was to provide a general methodology for practical application of the technology.

Summary and Research Need

The effects of corrosion and plastic deformation on the serviceable life of a structure is regularly studied with an aim to estimate the remaining capacity. Many models have been produced to do the same using finite element analysis software but the techniques employed require tedious manual work for modeling of the structure. In some cases, the estimation is based on the design plan, which does not accurately represent the as-built reality. Accurate in-situ geometric measurements are required for minimal error in remaining capacity calculations. LiDAR and photogrammetry have been studied in depth, and are used in structural engineering for various applications, one of which is deflection measurement. However, both techniques produce unwanted discrepancy or image noise, the effect of which needs to be studied.

Focus of this Thesis

The aim of this research is to prototype a standard methodology that can be used to quickly and effectively assess the capacity and state of stress of deficient structural elements using 3D imaging. 3D imaging techniques are used for accurate measurement of

damages and deformations, which are then used to undergo static stress analysis via finite element model updating. The proposed model updating approach dictates that the damages are isolated and modeled separately and then used to update an initial, undamaged model.

CHAPTER 3: SECTION LOSS SENSITIVITY STUDY

The first study proposed in the research evaluates the effect of image noise on the accurate creation of a finite element model. Using the photogrammetry techniques described in the previous chapter, a 3D point cloud can be generated for a given structural member. Using the 3D point cloud, a solid model can be created and then imported into FEM analysis software. The following sections further describe the process used in the study and subsequent analyses.

Ghahremani et al.'s Research

In a recent study, Ghahremani et al. proposed a systematic framework for section loss detection in structural components along with a validating experiment (Ghahremani, Lattanzi, and Khaloo). The study uses Dense Structure from Motion (DSfM) algorithms to capture detailed and dense point clouds of the surface of a member subjected to corrosion. The point cloud of the damaged surface was then compared with a point cloud of the initial model recorded previously. In absence of initial point cloud data, the point cloud was synthetically derived from 3D modeling of the as-designed geometry. The comparison of the two provided the differences that corresponded to section loss damages, which was further modeled into a solid body. This solid model of the damage was then used to update a finite element model of the initial condition by the Boolean operation of subtraction. The resultant model with section loss was then ready for finite

element stress analysis. Figure 1 shows a flowchart describing the steps in the model updating approach.

Goal of this Study

The study presented here explores the effect of image noise on the aforementioned model updating approach. Instead of comparing initial and final point clouds to retrieve damages and then modeling them, damages with varying degrees of artificial image noise were modeled from a synthetically produced point cloud. This produced solidified damages for updating the original model by subtraction, resulting in synthetically damaged plate specimens. These specimens were then imported into a finite element analysis software package. After assigning material properties, defining constraints and applying loads, the model was discretized, followed by static stress analysis under tensile loading.

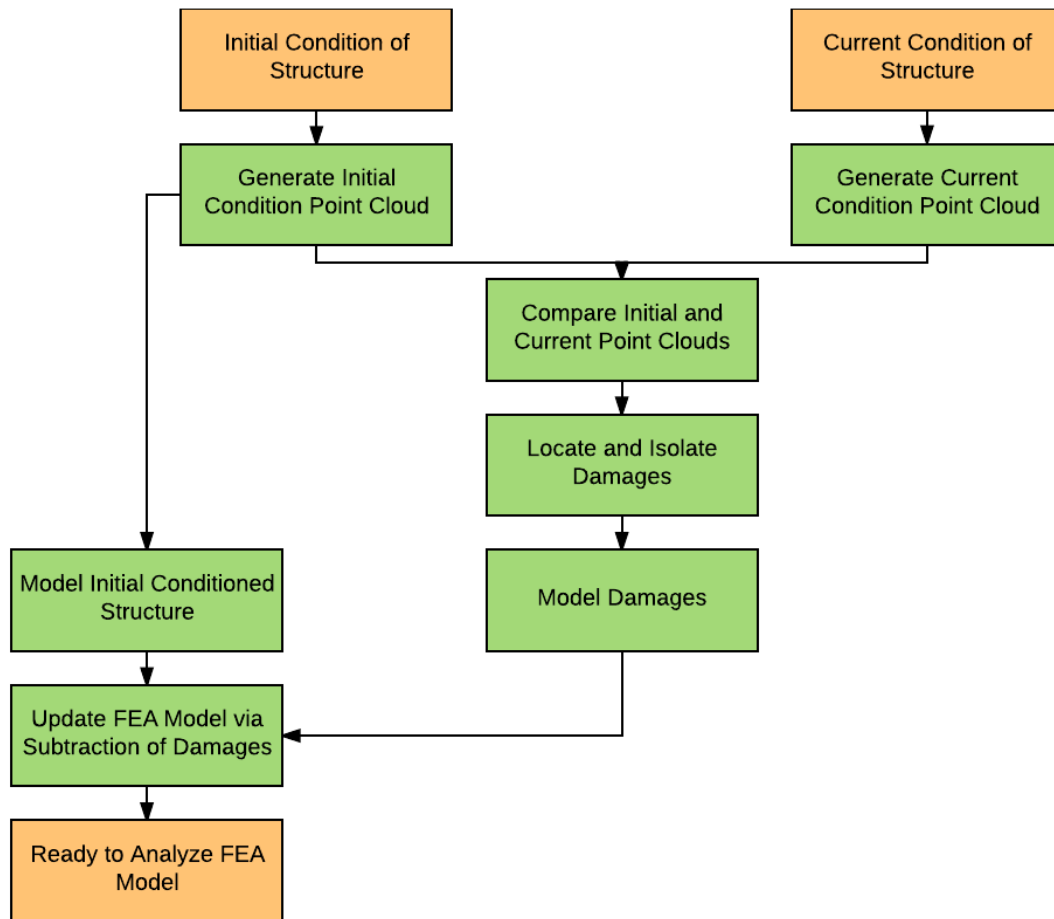


Figure 1: Ghahremani et al.'s proposed model updating approach for finite element analysis

Point cloud data inevitably comprises of some degree of background noise, which may be dependent on the instrument used, lighting, angle and reflective properties of the subject. This study was designed to correlate the effect of noise on the accuracy of the stress analysis measurements using Ghahremani et al.'s process. Uniaxial stress analysis was performed on twelve separate plate specimens in Autodesk Inventor, each with a hole cut out of the center of 12 inch by 3 inch plates with 1/4-inch thickness. These holes represented section loss due to corrosion that would cause a stress concentration to arise.

Nine of the twelve plates were prepared from modeled meshes of artificial point clouds which were then subtracted or cut from the plate. The remaining three specimens were created by cutting 'pure' holes in the plates in Inventor as control specimens that incorporate no image noise or modeled artifacts.

Methodology

The first step was to create synthetic point clouds of damage, recreating step 4 of Ghahremani et al.'s flowchart in Figure 1. The synthetic holes were essentially cylindrical in shape, with 2 faces: front and back, and the wall of the cylinder. The size of the hole was denoted by the diameter of its front or back face. The thickness of the hole was the length of the cylinder. Three different sized holes were created with diameters of 0.5, 1.0 and 1.5 inches; each of which were associated with three degrees of noise: 0%, 10% and 25%. The percentage is a representation of the proportion of the diameter that was added around the edge of the initial diameter as random white noise along the length wall of the cylinder which was a standard 0.3 inches long for all specimens. A MATLAB (MATLAB R2015a) script was written to generate artificial point clouds for the 9 types of holes. The MATLAB script generated point clouds containing 15,000 points, 5000 points for each face of the cylinder and 5000 for the wall of the cylinder. Starting at origin, the script would arbitrarily cycle through the selected radii and cylinder heights to give each point a distinct X, Y and Z coordinate. The degree of image noise was included by allowing the script to overestimate the diameter of the hole by 0%, 10% and 25% depending on the case considered. Figures 2 & 3 show the dimensions of these point clouds.

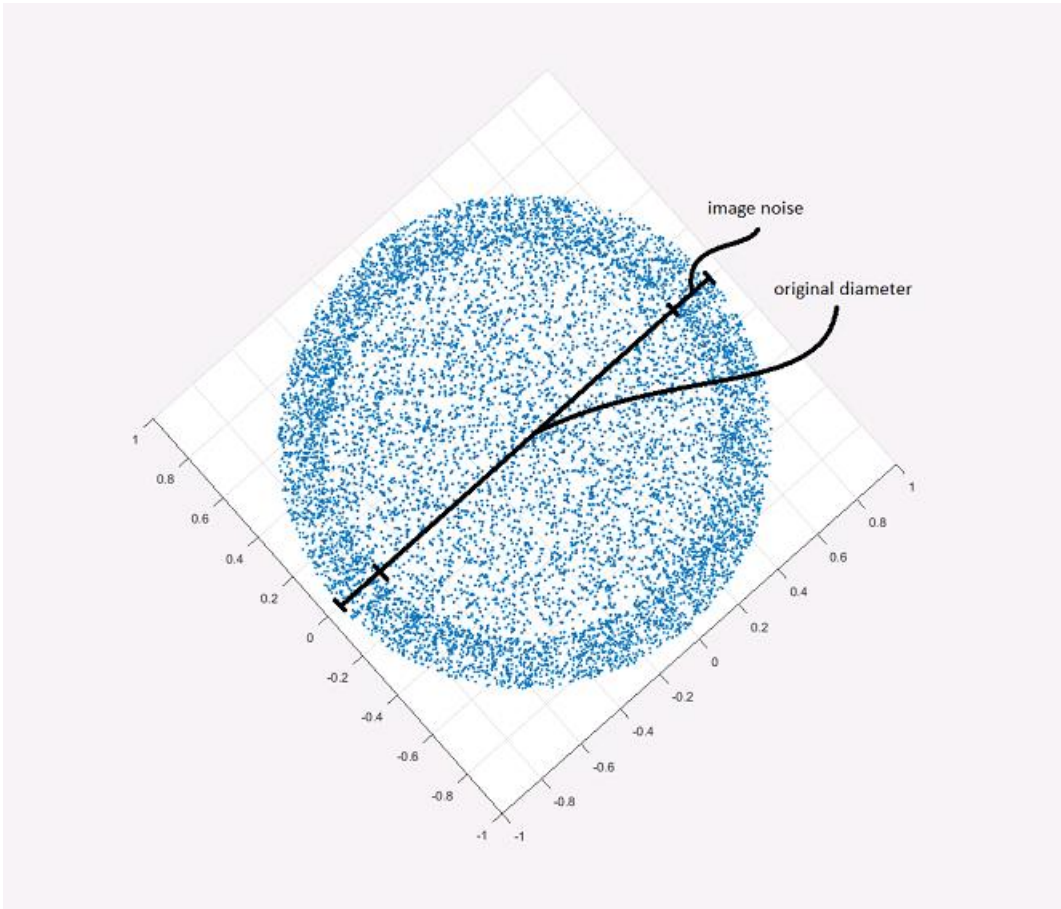


Figure 2: Face view of point cloud for 1.5" diameter hole with 25% image noise

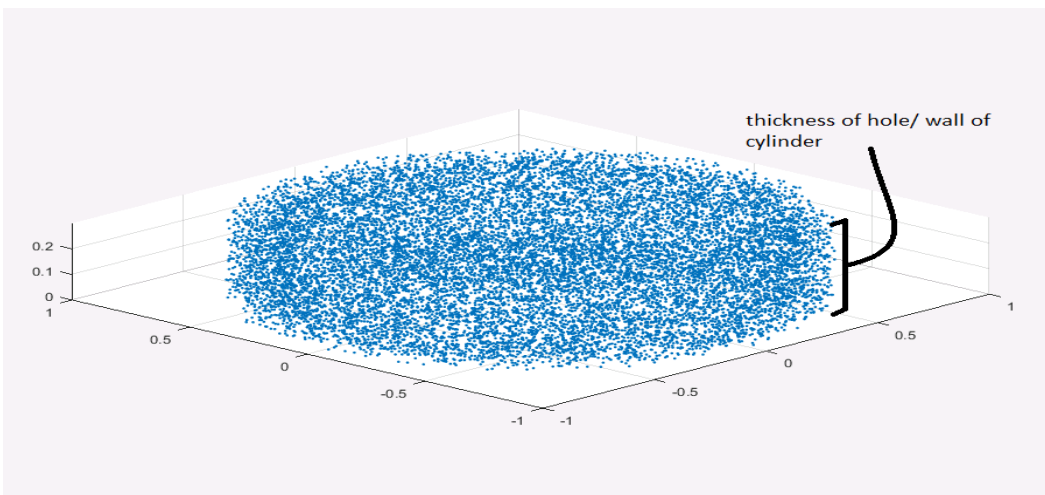


Figure 3: Side view of 1.5" diameter hole with 25% noise

The nine clouds generated from MATLAB contained the point cloud information in the form of 3D coordinates. To mesh the point clouds, each file was imported individually into MeshLab (MeshLab), an open source software package designed to work with point cloud data. An imported point cloud can be seen in Figure 4(a). Meshing the clouds require the calculation of normals to the point sets and their orientation. The normals for the point cloud were estimated based on a specified number of neighbors for each point, 16 in this case. Once the normals were computed, the Poisson surface reconstruction algorithm was used to generate a surface mesh (M. Kazhdan, Bolitho, and Hoppe). This algorithm delivers a wire mesh consisting of triangular elements that form a watertight surface that can be readily modeled into a solid 3D object. Figure 4(b) also shows the resulting surface wire mesh for the imported point sets. In this algorithm, octrees are used to control mesh detail and refinement. An octree depth of 5 was selected to achieve scalable results at the cost of some accuracy and detail. The number of faces and vertices was considerably reduced, condensing the size of the meshed models. The meshes were then exported to AutoCAD (Autodesk AutoCAD) as DXF files and converted to DWG format.

The DWG files were then imported in Inventor (Autodesk Inventor) to create a 3D sketch with surfaces and wires. Once imported, Inventor produced a polygon mesh, a network of triangular faces made from edges and vertices. The ‘Stitch’ command converted the 2D surfaces into a composite solid body. This process can be memory intensive, dependent on the number of nodes and elements as well as the maximum tolerance allocated. A larger maximum tolerance can produce quick results at the cost of

accuracy. A maximum tolerance of 0.1 inches was used in this study. The solidified hole was then saved as a standard part file in Inventor as can be seen in Figure 5(a).

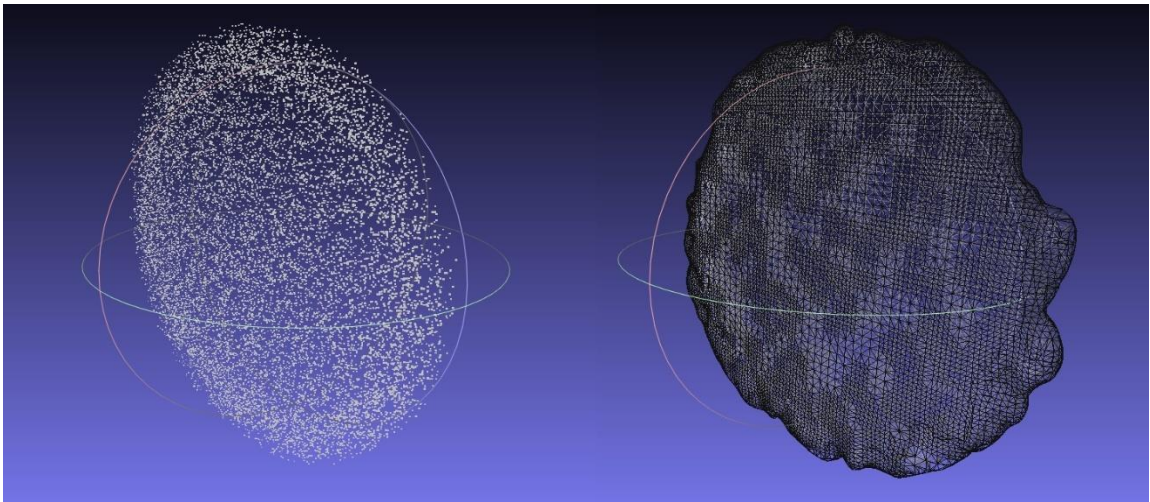


Figure 4: (a) Imported point cloud (left) and (b) associated wire mesh (right) in MeshLab

A quarter inch thick solid plate was then created in Inventor with a length of 12 inches and cross-section of 0.25 by 3 inches. A new inventor assembly was created and the plate and the hole part files were introduced using the ‘Place’ command. After orienting the hole at the center of the plate through its cross-section, the plate was selected as a surface but not associative. This created a copy of the hole in the exact same position and was then subtracted from the plate. Figure 5(b) shows the resulting section loss. Then damaged plate was saved as a part file. The process was repeated for all holes to generate plates with holes to emulate section loss due to corrosion.

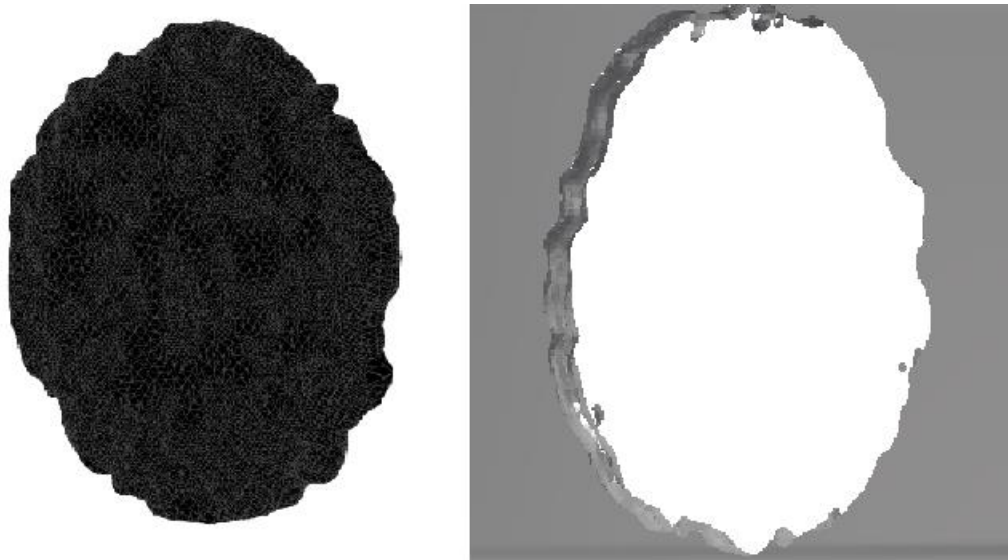


Figure 5: (a) Solid model of damage (left) and (b) plate specimen updated by subtracting the damage

Surface reconstruction and meshing may cause a loss of detail and integrity of the data. This occurs due to the fitting of the points to the surface and leads to smoothing of the mesh, especially at locations of minor damages. Hence, another 3 models were created in Inventor with holes of the 3 sizes cut out so as to produce sections with ‘pure’ cylindrical holes. These specimens were produced in the same manner as the plate itself and served as experimental controls. Figure 6 shows the differences between the holes of same original diameter, but with different noise levels, subtracted from the plates. The top left image is that of a pure section loss. The top right image is that of a point cloud based hole with 0% image noise; though, the two holes have no noise, some discrepancy is visible in the point cloud hole. The bottom images are of holes with 10% and 25% image noise respectively.

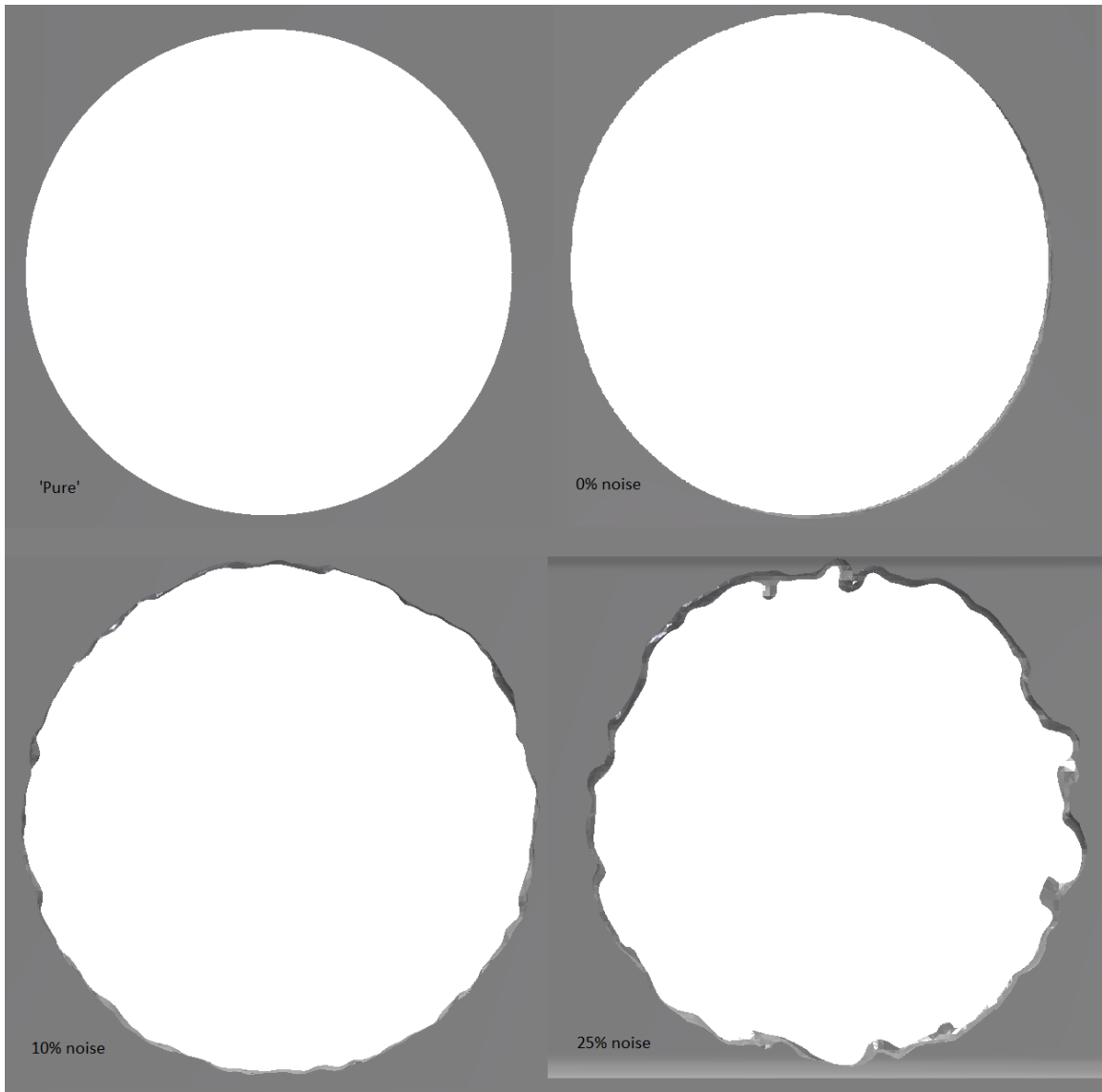


Figure 6: 1.5" diameter holes with various levels of noise

Analysis

A static stress analysis was then performed in Inventor on each of the models. ASTM A36 steel was chosen as the material for all tests. For the tension test, a 10-kip load was distributed at each end face. Vector component constraints were used to emulate pin connections at the center of the top & bottom surfaces by restricting movement in the

x, y and z directions. Similarly, a roller connection was imitated by constricting translations in y and z directions. See Figure 7 for more details.

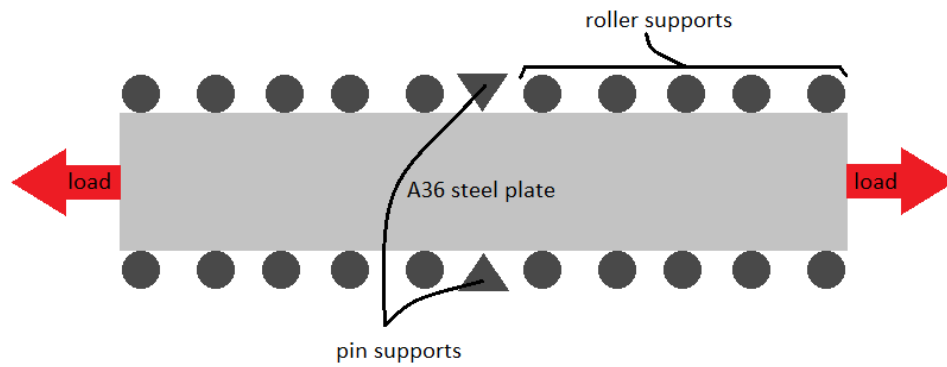


Figure 7: Tensile test model schematic

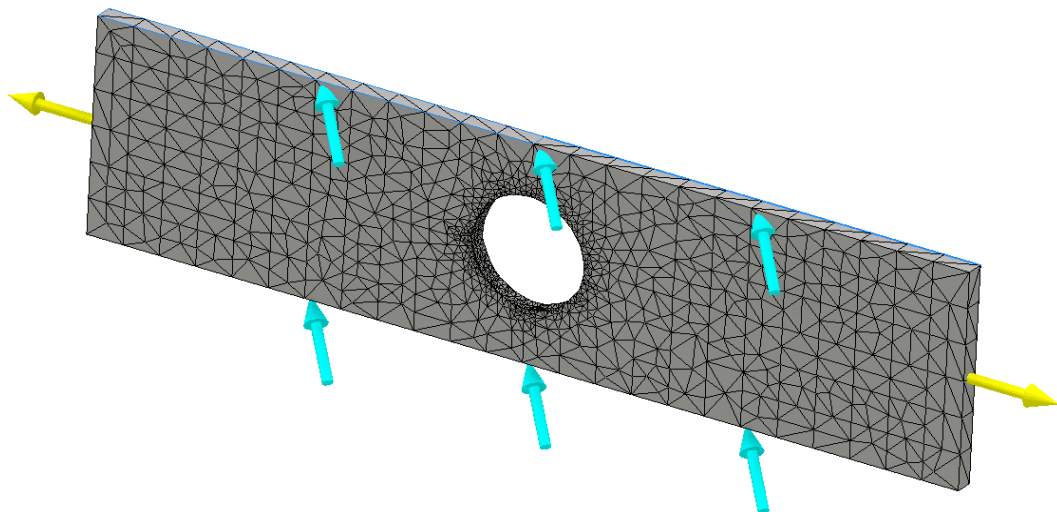


Figure 8: Ready-to-analyze section loss specimen in Autodesk Inventor

Once modeling was completed, each plate specimen was meshed (discretized) and simulation was performed. A discretized specimen is shown in Figure 8 under axial tension with constraints. The yellow arrows indicate the axial loads of 10kips. The blue arrows indicate the constraints to imitate pin and roller supports. The time duration of the finite element analysis depended on the size of the mesh and the number of elements and nodes. Figures 9 and 10 show the calculated von Mises's stress profile for one specimen; with probes that indicate key locations for stress estimation. The max stresses found at the surface of the hole were recorded. Additional stresses were manually recorded using probes, as seen in Figure 10, including stresses just below the surface of damage at approximately one-eighth of an inch and at the extreme bottom fiber.

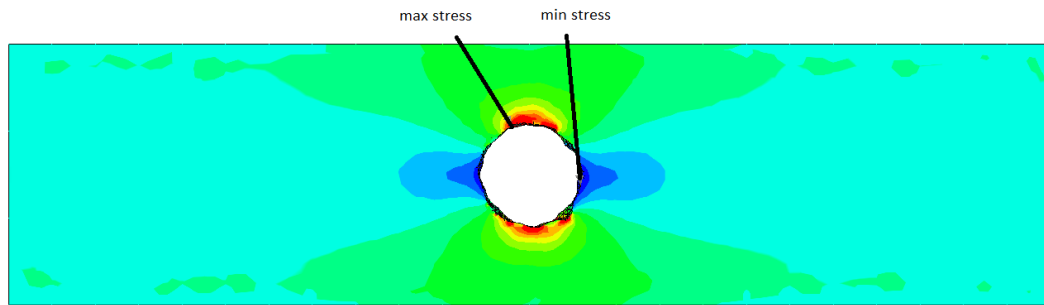


Figure 9: Von Mises stress profile of 1.0" diameter hole specimen with 25% noise

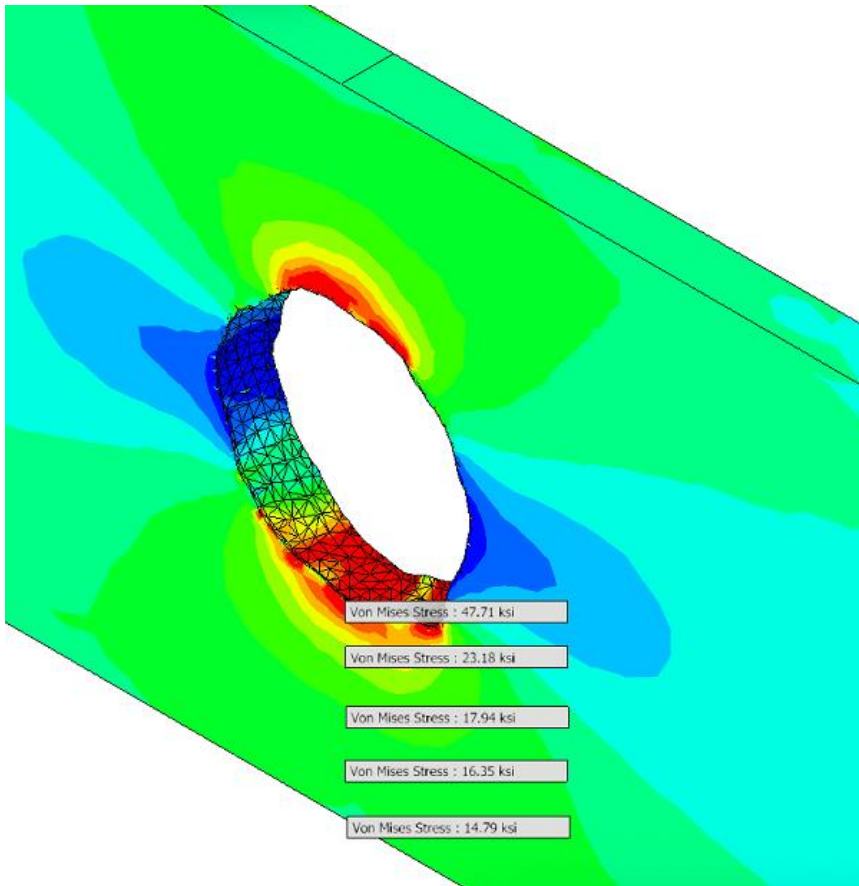


Figure 10: Key locations for stress estimation

Results

Stress concentrations tend to develop near regions of rapidly changing geometry. In the cases studied in the research, a natural stress concentration developed at the surface of the damaged hole in accordance with classical elasticity analysis, since the surface had many flaws due to the corrosion with a potentially jagged and unpredictable geometry. Due to the finite element formulation, the nodes at these sharp features indicated a maximum von Mises stress that is unrealistically high and not representative of the actual stress in the material due to localized plasticity. Therefore, the research not only reports

the maximum stress recorded, but also reports the stress below the hole surface at an approximate distance of 1/8 inch away to provide a better understanding of the anticipated maximum stress.

Table 1 lists the results of the static analyses as Von Mises's stresses of the plates emulating section losses due to corrosion of various sizes and noises. Max stresses are also recorded and compared with the subsurface stresses near the holes to calculate a percentage difference.

Table 1: Observed maximum stresses and stresses below damaged hole surface, and their percentage difference

Specimen No.	Specimen Detail	Max Stress (ksi)	Stress Below Hole Surface (ksi)	Percentage Difference (%)
1	0.5" 'pure' cut with 0% noise	34.27	32.43	5.67
2	0.5" modeled with 0% noise	42.67	34.96	22.05
3	0.5" modeled with 10% noise	60.73	33.24	82.70
4	0.5" modeled with 25% noise	60.93	35.38	72.22
5	1.0" 'pure' cut with 0% noise	36.00	35.49	1.44
6	1.0" modeled with 0% noise	50.28	38.64	30.12
7	1.0" modeled with 10% noise	59.62	42.42	40.55
8	1.0" modeled with 25% noise	77.15	47.71	61.71
9	1.5" 'pure' cut with 0% noise	41.70	41.25	1.09
10	1.5" modeled with 0% noise	65.52	47.16	38.93
11	1.5" modeled with 10% noise	58.93	50.74	16.14

12	1.5" modeled with 25% noise	201.90	43.70	362.01
----	-----------------------------	--------	-------	--------

From Table 1 it can be inferred that the max stresses, when compared with stresses even a fraction of an inch below the surface, can differ significantly. It was also observed that these max stresses always occur at the surface of the damaged area, due to a local stress concentration effect. These locations are mostly sharp edges or points, which occur when the smoothed surface of the modeled holes or damages are subtracted via Boolean operation from the plate as illustrated in Figure 11.

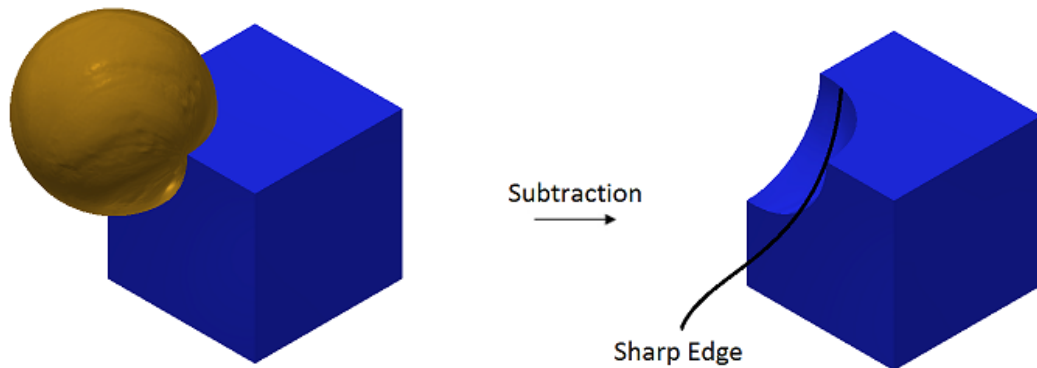


Figure 11: Sharp edges and pointed locations after subtraction

Figure 12 is a plot of the max stresses observed at the damaged surface for the various specimens. It clearly indicates an expected rising trend in these max stresses as the amount of random image noise increases from 0% to 25% for all sized holes. There is

also a similar difference between the ‘pure’ cut section loss and the modeled 0% noise hole. This is because of the modeling algorithm. Even with a point cloud with no image noise, the modeling process tends to induce irregularities that create sharp edges and points, and cause an increase in max stresses due to stress concentrations.

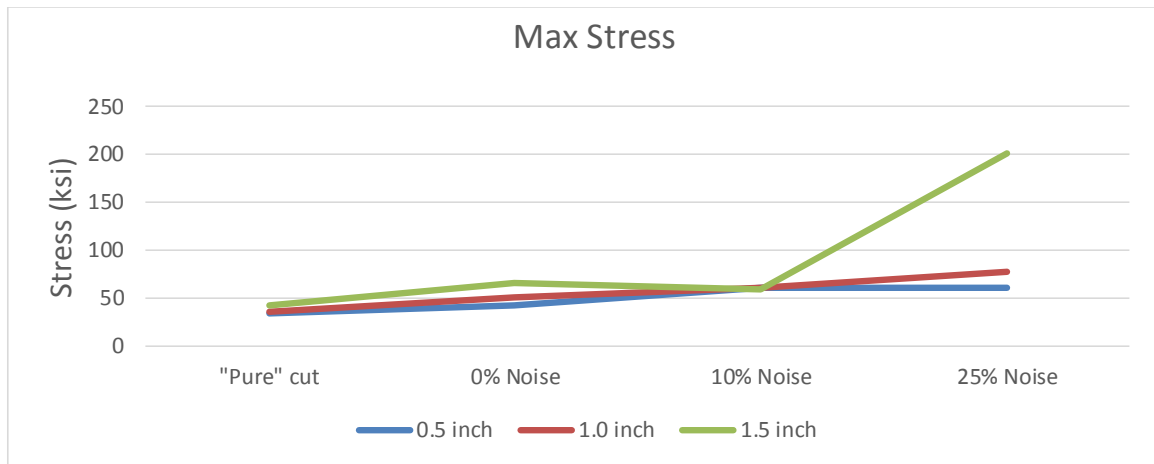


Figure 12: Line graph of max stresses observed

The rule of stress concentration effect dictates that for a circular hole in the center of a plate under uniaxial tension, as in Figure 13, the stresses observed at point B are related to the remote stresses at point A by a multiplier. This multiplier is known as the stress concentration factor. Based on analytical predictions, it ranges from 3.0 to 2.0 depending on the dimensions of the hole and the plate. When the ratio of the diameter of the hole, d , to the width of the plate, W , approaches zero the stress concentration factor becomes 3. It decreases asymptotically towards 2 as the ratio, d/W , increases to unity.

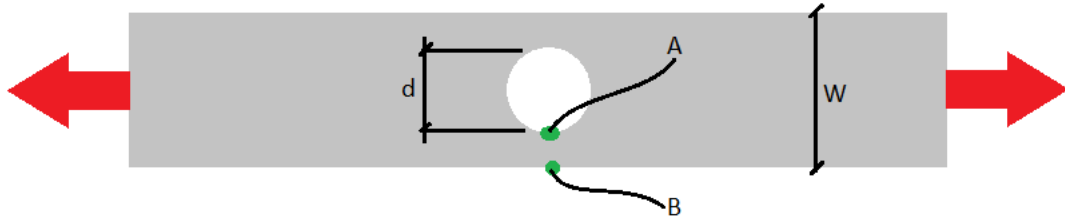


Figure 13: Diagram of axial specimen for stress concentration factor calculations

The stress concentration factor for this study is calculated as the ratio between the max stress found just below the surface of the damage and the remote stresses at the bottom fiber of the plate. Table 2 presents the predicted stress concentration factor from the chart in Figure 14 and the observed value from the experiments. It can be inferred that the average observed value for the four 0.5-inch diameter specimens is 3.05 which differs from the predicted by 19%. Similarly, the averages of 1.0 and 1.5-inch specimens are 3.07 and 2.49 in contrast to the predicted value of 2.35 and 2.19; a percentage difference of 30.6% and 13.7%.

Table 2: Stress concentration factor comparison

Specimen No.	Specimen Detail	Stress Below Hole Surface (ksi)	Stress at Bottom Fiber (ksi)	D/W	Stress Concentration Factor	
					Predicted	Observed
1	0.5" 'pure' cut with 0% noise	32.43	10.87	0.17	2.57	2.98
2	0.5" modeled with 0% noise	34.96	11.7	0.17	2.57	2.99

3	0.5" modeled with 10% noise	33.24	11	0.17	2.57	3.02
4	0.5" modeled with 25% noise	35.38	11.1	0.17	2.57	3.19
5	1.0" 'pure' cut with 0% noise	35.49	12.6	0.33	2.35	2.82
6	1.0" modeled with 0% noise	38.64	12.79	0.33	2.35	3.02
7	1.0" modeled with 10% noise	42.42	13.2	0.33	2.35	3.21
8	1.0" modeled with 25% noise	47.71	14.79	0.33	2.35	3.23
9	1.5" 'pure' cut with 0% noise	41.25	14.89	0.50	2.19	2.77
10	1.5" modeled with 0% noise	47.16	17.77	0.50	2.19	2.65
11	1.5" modeled with 10% noise	50.74	19.28	0.50	2.19	2.63
12	1.5" modeled with 25% noise	43.7	23	0.50	2.19	1.9

Noise Analysis

As previously discussed, the synthetic point clouds for holes were generated with random white noise using a MATLAB algorithm. By design, the consistency of which could not be controlled, and the randomness of point generation could cause a local concentration of points. This bias led to modeling of unexpected artifacts with erroneous maximum stresses. An analysis on the randomness of noise generation was completed. The selected specimen size was 1.0-inch diameter hole with 25% noise. Ten separate point clouds were created from the MATLAB script, and similarly modeled and used to update the initial plate. The specimens were then analyzed and the recorded results are tabulated in Tables 3 and 4.

Table 3: Stresses observed from analysis of 10 specimens

Specimen No.	Max Stress (ksi)	Stress Below Hole Surface (ksi)	Percentage Difference (%)
1	92.39	39.83	131.96
2	93.83	45.17	107.73
3	115.60	39.50	192.66
4	149.51	54.06	176.56
5	121.60	46.10	163.77
6	97.20	39.01	149.17
7	102.10	40.70	150.86
8	128.80	47.10	173.46
9	106.30	45.62	133.01
10	127.20	51.76	145.75

Table 3 shows that the max stresses found at the surface of the damages differ from the stress below the surface of the hole by an average of 153%. It should be noted that the specimen 12 from Table 1 is now considered an outlier. The percentage difference for that specimen was 362%. Table 4 compares the predicted stress concentration factor (Richard G. Budynas) with the observed. It can be observed that the average stress concentration factor of 1.98 is close to the stress concentration factor predicted for the specimen.

This study proved that the von Mises's surface stresses observed are due to the artifacts and do not represent the actual state of stress. Hence, these should be ignored. The highest stress found under the damaged surface show the true state of stress for the plates. This information can be utilized to evaluate remaining capacity of the plates and in further research using the finite element model updating approach.

Table 4: Stress concentration factor comparison for 10 specimens

Specimen No.	Stress Below Hole Surface (ksi)	Stress at Bottom Fiber (ksi)	D/W	Stress Concentration Factor	
				Predicted	Observed
1	39.83	22.64	0.50	2.19	1.76
2	45.17	22.68	0.50	2.19	1.99
3	39.50	23.81	0.50	2.19	1.66
4	54.06	24.18	0.50	2.19	2.24
5	46.10	21.83	0.50	2.19	2.11
6	39.01	20.08	0.50	2.19	1.94
7	40.70	22.95	0.50	2.19	1.77
8	47.10	22.44	0.50	2.19	2.10
9	45.62	22.26	0.50	2.19	2.05
10	51.76	23.67	0.50	2.19	2.19

CHAPTER 4: DEFLECTION STUDY

The second study proposed in the research utilizes the deflection measurements to update a finite element model and analyze its state of stress. Using the photogrammetry techniques described in chapter 2, a 3D point cloud can be generated for a given structural member before and after deflection. Using the two 3D point clouds, the deflections at certain location are measured and then imported into a finite element model analysis software. The following sections further describe the process used in the study.

Jafari et al.'s Research

The study by Jafari et al. was concerned with deflection measurements based on point clouds. The experiment involved three-point bending tests of aluminum bars of various thicknesses. The research successfully led to extraction of deflection measurements. In this research, 12 by 1 inch aluminum bars of 1/8 and 1/4 inch thicknesses were used. The bars were deflected under a three-point bending test equipment. The bars were marked at inch intervals from 2 to 10 inches. Photographs taken during the tests were used to generate point clouds of the specimens using DSfM, as discussed in chapter 1. After filtering and aligning the point clouds, an algorithm was run that would estimate the deflections between the two bars at specific intervals. The distance between the nearest neighbors of the selected correspondence points from both point clouds are calculated (Jafari, Khaloo, and Lattanzi).

Goal of this Study

The main objective of the deflection study performed in this study was to quantify the extracted measurements from photogrammetric methods into a state of stress for the bars, which will help in remaining capacity evaluation. A model for the un-deflected bar was created and then updated with the recorded measurements obtained using close range photogrammetry. By measuring the differences in the associated point cloud data, a deflection analysis could be performed in the finite element software on the bar forced into the measured deformed shape. Subsequently, a static stress analysis was completed to achieve the bending stress profiles for the specimens.

Methodology & Analysis

This study involves data collected by Jafari et al. In this research, 12 inch by 1 inch aluminum bars of 1/8 inch and 1/4 inch thicknesses were used. The bars were deflected under a three-point bending test equipment. The bars were marked at 1 inch intervals from 2 to 10 inches along the length of the bar. Photographs taken during the tests were used to generate point clouds of the specimens using DSfM, as discussed in chapter 1. After filtering and aligning the point clouds, an algorithm was run that would estimate the deflections between the two bars at specific intervals. The distance between the nearest neighbors of the selected correspondence points from both point clouds are calculated.

The aim of this study was to utilize the measured deflections to produce a bending stress profile by inducing translation in an associated finite element model. The bars were modeled in Autodesk Inventor for finite element analysis. The measured deflections along the length of the bars were used to force vertical translation at respective locations

for each bar as tabulated in Table 5. Aluminum was assigned as the material from the Autodesk material library. No loads were applied as the aim was to understand the state of stress for a measured deflected shape. The bar was supported at 2 inches from either ends, leading to an 8-inch span length.

Table 5: Measured deflections and applied load (Jafari et al.)

Specimen Details	Measured Deflections at Marked Locations (in)								Load (kips)
	0	1	2	3	5	6	7	8	
1/8" thick	0.000	-0.078	-0.135	-0.198	-0.186	-0.156	-0.078	0.000	0.032
1/4" thick	0.000	-0.117	-0.118	-0.124	-0.118	-0.115	-0.062	0.000	0.250

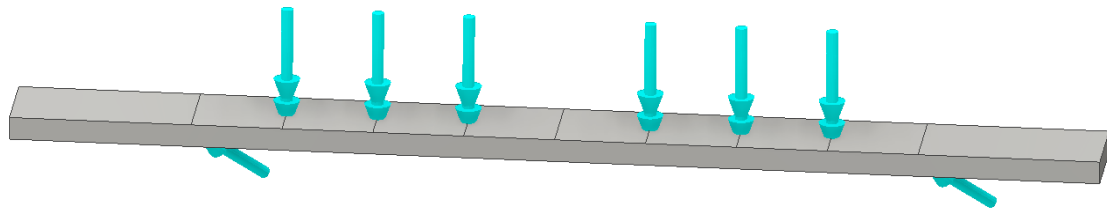


Figure 14: FEA model for deflection study

Figure 14 shows the assembly for a bar in Autodesk Inventor with applied displacements. The blue double arrows on the top indicate the induced translations as calculated previously. As can be seen, the center of the bar lacks any such translation because during the process of DSfM it was deemed an inaccurate measurement point due to the load applied using the equipment, and deflections could not be measured at that location. The single arrows on the bottom of the bar indicate the applied constraints that

imitate the pin and roller supports at 2 and 10 inches from the left bar end. The specimen was then discretized and analyzed.

Results

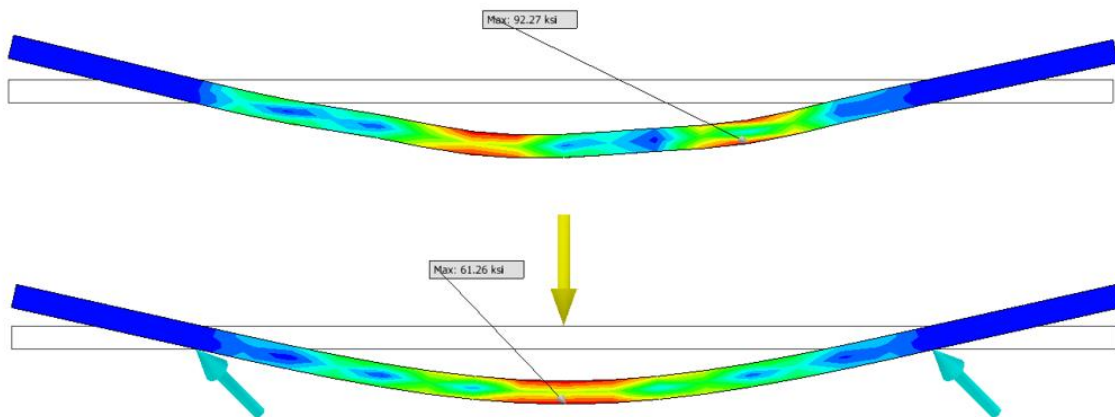


Figure 15: General stress profile results: (a) due to induced load (top) and (b) due to applied point load (bottom)

Figure 15 shows the observed (top) and predicted stress profiles for a 1/8-inch thick bar under a 32-pound point load (bottom). The observed stresses result from the induced deflection experiment. The predicted results are generated by applying the recorded point load from the earlier experiment, as listed in Table 5. Euler-Bernoulli beam theory results for the same load are also calculated. The results are tabulated for both specimens in Table 6. The results were not as expected. For the purpose of comparison, the maximum stresses that were not found at mid-spans of the specimens are not used as they do not reflect the true state of stress and only occur due to the stress concentration effect. The stress concentrations are a result of the localized displacements that were applied. Instead, the observed mid-span stresses are used. For the 1/8-inch thick

bar, the max stress observed is 8.74ksi as compared to the analytical calculation of 25ksi from Euler-Bernoulli bending theory, a 186% difference. For the 1/4-inch bar, the observed stress is 3.7ksi and expected was 48ksi, a percentage difference of over 1000. The reason behind the low stresses observed is because at mid-span there is not displacement induced and the bar is essentially straight.

Table 6: Max stresses observed for specimens

Specimen No.	Specimen Details	Load (kips)	Mid Span Stresses (ksi)			Max Stress by Induced Deflection (ksi)
			Induced Deflection	Point Load	Euler Bernoulli Theory	
1	1/8" thick	0.032	8.74	24.52	24.58	48.94
2	1/4" thick	0.250	3.70	47.88	48.00	210.90

The study shows that when localized displacements are applied to induce vertical deformation of the bar, a stress concentration develops at the applied locations in a 3D state of stress. Due to this phenomenon, the maximum stresses observed do not represent the actual state of stress, disproving this deflection analysis as an accurate way to update the finite element model. This study also indicates that displacement is a continuous phenomenon; only a curve of the deflected shape or measured deflections at minute distances would prove useful in 3D stress estimation.

CHAPTER 5: CHALLENGES & LIMITATIONS

As the point clouds generated in MATLAB were random, there was no certainty where the generated points produced would accumulate. Hence, a noise analysis on the randomness of point cloud generation was completed. A standard density could not be managed throughout the synthetic damaged regions and experimental repeatability was limited. From the results we learnt that random point generation could cause accumulation of synthetic noise in some areas. This caused the modeling algorithm to produce artifacts here, because of which the max stresses can vary in a wide range. This issue escalated with the size of the hole in question, because various levels of noise were designated as a percentage of the diameter added to the original hole. A 1.5-inch hole with 25% noise had an additional 0.375 inches to its diameter where the synthetic noise occurred. A 0.5-inch hole would have only 0.125 inches. This provided the bigger hole with more area where synthetic image noise could be generated randomly, thereby decreasing the uniform density of the points, as compared to a smaller hole of same noise level. This can be seen below in Figure 16; the red area indicates the area where noisy points were generated. It is considerably larger for the 1.5-inch hole as compared to the 0.5-inch hole.

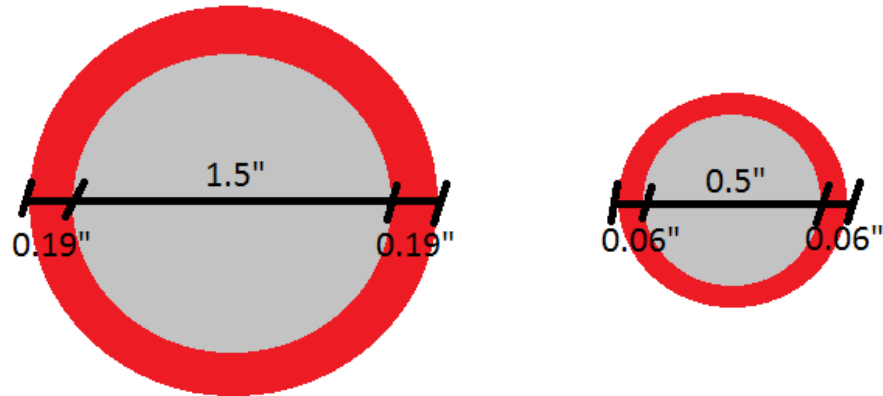


Figure 16: Holes of sizes 1.5" and 0.5" with 25% noise

Moreover, the fine detail of the meshed hole is dependent on a number of factors when using the surface reconstruction algorithm. Originally octree depths of 8 and 6 were used producing highly accurate meshes, but with a large number of faces and vertices. The process of subtraction left many local surface reconstruction artifacts on the plates. Hence, when discretizing for finite element analysis the number of elements would increase beyond the allowed capability of Inventor due to licensing limitations. Eventually, a lesser detailed octree depth of 5 was used, which smoothed out the finer details. Figure 17 shows the holes meshed using different octree depths. Time consumed versus accuracy demanded is a tradeoff that could be adjusted in future work.

The generation of point clouds, the meshing and modeling of the damage and the process of subtraction and discretization are all interrelated. Any anomalies in the point clouds are carried forward in the surface mesh and the FEA model. It is difficult to isolate the impact of each step on the FEA modeling results.

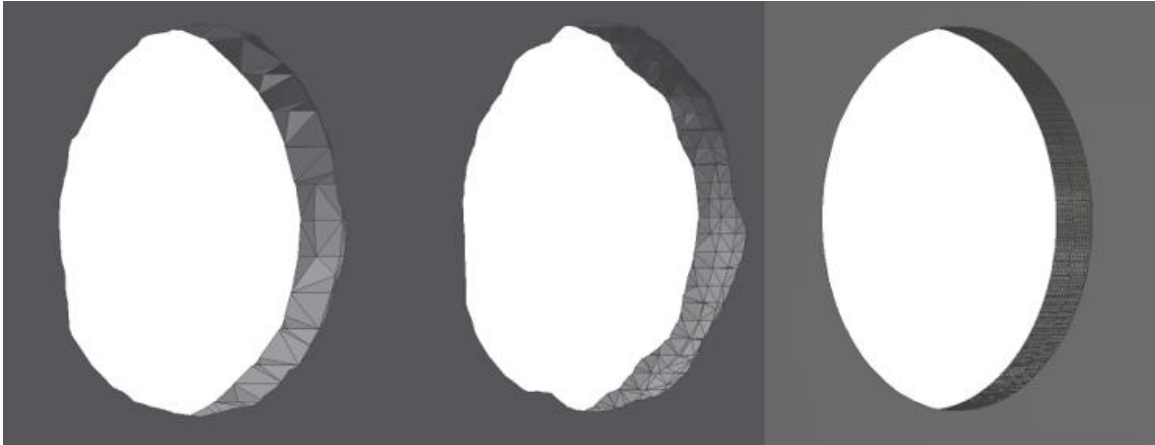


Figure 17: Holes meshed using octree depths of 5, 6 and 8 (from left to right)

In the section loss sensitivity study, we can associate the observed high stresses with image noise mainly because we know what result to expect according to the well understood stress concentration effects for circular holes. However, if the section loss is arbitrary, it becomes more difficult to distinguish noise artifacts from real stresses. We know that they would normally arise at sharp transitions on the model surface so it is recommended to neglect all surface stresses and look for subsurface peaks in future studies.

Similarly, the noise captured in the point cloud is hard to distinguish from the actual surface of the subject. This is dependent primarily on the resolution of the instrument. LiDAR generates high density and consistently distributed point clouds. However, photogrammetric images are dependent on the instrument as well as the lighting, the angle of incidence and the reflection properties of the subject. The DSfM

algorithm used could easily incorporate background noise. This is true especially for small damages, like cracks, where the presence of noise will play a vital role.

These experiments were based on the assumption that the material remains in the linear elastic zone. However, the stresses observed were higher than the yield strength of the material, A36 steel. Plastic deformation of damages and deformations, if accounted for would reduce the peak stresses found at artifacts. In that case the sharp edges will experience elongation; an increase in area will accommodate more stress. Autodesk Inventor does not allow non-linear static analysis.

CHAPTER 6: CONCLUSION

The purpose of this research was to prototype and investigate a methodology of using 3D images for capacity analysis of damaged structural elements, either with section loss or under deformation, using a newly developed finite element model updating approach. This approach dictates that damages are isolated by comparison of original and damaged point clouds, generated through terrestrial laser scanning or photogrammetry. Isolated damages are then used to update an initial model and analyzed accordingly.

The section loss study used synthetically produced isolated point clouds of circular section loss with random image noise of various amplitudes. The points were meshed together to form a surface mesh using a surface reconstruction algorithm. The wire mesh was then modeled in Inventor and solidified into a 3D model of the damage. Using the Boolean operation of subtraction, the modeled hole was cut out from the original plate and produced a specimen with section loss. The specimens were then analyzed using finite element analysis package to quantify the effect of image noise on the measured stress levels of the plate under tensile load. This experiment also enabled exploration of the overall technique of Ghahremani et al and identification of its limitations.

The results indicated that with increase in image noise the max stress found at the surfaces of holes increased. This is because the number of sharp edges and dislocations in

the mesh increased. These stresses were deemed to be modeling artifacts and did not represent the true state of stress. However, just below the damaged surface, simulated stresses followed expected stress concentration effect for circular holes. The stress concentration factor for the specimens were found in the range of 2.0 to 3.0, as expected. The process of meshing and modeling themselves also induced artifacts, as shown by the higher max stresses observed in the modeled hole of 0% noise as compared to ‘pure’ cut holes from Inventor.

The deflection study utilized the deflection measurements recorded from point cloud comparisons captured by photogrammetry during the three-point bending tests. The deflections observed were induced in a finite element model of the bars to produce vertical translation. The deformed bars were then discretized and analyzed. The observed stress profiles were compared with the expected stress levels predicted by beam theory. Unfortunately, the two differed greatly and any conclusive correlation was not possible. The reason for the high observed stresses was due to the application of localized displacements which caused local stress concentrations.

Future Work

There is a definite need for further research to make this approach more practical. To do so a number of studies are recommended.

One-dimensional beam elements could be used in the deflection study. As the major concern in the induced deflection experiment is the local stress concentration, a “stick” model can be used which would essentially eliminate the stress concentration effect. This is because any 2D or 3D states of stresses are ignored in the process. Similar

to this study, the model would be forced to deform using the measured deflections. The resulting bending moments and shear stresses can be recorded. The rotations and deflections can then be used to calculate the observed max stresses. Even though a stress profile is not produced, the aim of calculating the remaining capacity of the beam can be fulfilled.

Another recommendation would be to calculate a curve that represents the continuous deflection of the bars. This curve can then be used to emulate the deflected shape of the bar in an FEA package. Doing this will eliminate any local stress concentration effect, because the applied deflection will be smooth.

A convergence analysis on the finite element model should be undertaken to understand how meshes of different density and complexity affect the obtained results. We know that the accuracy and level of meshing detail is controlled by the octree depth for the surface reconstruction algorithm. A study could be designed to explore the differences in resulting stress profile from different octree depths. Moreover, the study could also provide insight on to what level of meshing detail is acceptable with regard to time consumed and accuracy lost.

More sophisticated finite element modeling software can be used, providing more extensive control over the discretization analysis processes. Furthermore, the use of a non-linear static analysis as compared to Inventor would be beneficial. The effect of plastic behavior of the material on the otherwise artificial peak stresses can also be studied. This will provide more insight on the stress concentration effect and will provide more reliable results.

Field study will also provide further insight on the effects of actual background image noise as compared to the synthetically induced noise used in the section loss sensitivity study. The use of de-noising and filtering algorithms can also be studied in that case.

Actual corroded beams with arbitrary section loss need to be studied with experimental validation to further explore the accuracy of the model updating approach and its use for remaining capacity analysis.

Other methodologies regarding capacity and remaining life estimation discussed in the literature review need to be considered. The model updating approach can be merged with these techniques to perform analysis. A comparative study will yield a practical and reliable process.

REFERENCES

- Armesto, Julia et al. “FEM Modeling of Structures Based on Close Range Digital Photogrammetry.” *Automation in Construction* 18.5 (2009): 559–569. *ScienceDirect*. Web.
- AutoCAD. San Rafael, CA: Autodesk Inc.
- Barbieri, Gaia et al. “Assessing the Seismic Vulnerability of a Historical Building.” *Engineering Structures* 57 (2013): 523–535. Print.
- Cabaleiro, M. et al. “Algorithm for Beam Deformation Modeling from LiDAR Data.” *Measurement* 76 (2015): 20–31. *ScienceDirect*. Web.
- Conde-Carnero, B. et al. “Exploitation of Geometric Data Provided by Laser Scanning to Create FEM Structural Models of Bridges.” *Journal of Performance of Constructed Facilities* (2015): 04015053. Print.
- Czarnecki, Artur A., and Andrzej S. Nowak. “Time-Variant Reliability Profiles for Steel Girder Bridges.” *Structural Safety* 30.1 (2008): 49–64. *CrossRef*. Web.
- F Laefer, Debra, Linh Truong-Hong, and Michael Fitzgerald. “Processing of Terrestrial Laser Scanning Point Cloud Data for Computational Modelling of Building Facades.” *Recent Patents on Computer Science* 4.1 (2011): 16–29. Print.

- Ghahremani, Kasra, David Lattanzi, and Ali Khaloo. "Automated 3D Image-Based Section Loss Detection for Finite Element Model Updating." 33rd International Symposium on Automation and Robotics in Construction, 2016. Print.
- Guarnieri, Alberto et al. "Combined 3D Surveying Techniques for Structural Analysis Applications." *International archives of photogrammetry, remote sensing and spatial information sciences* 36.5/W17 (2005): 6. Print.
- Guldur, Burcu, Yujie Yan, and Jerome Hajjar. "Condition Assessment of Bridges Using Terrestrial Laser Scanners." *Structures Congress 2015*. American Society of Civil Engineers. 355–366. ASCE. Web. 8 Oct. 2015.
- Hartle, R. A., and Federal Highway Administration. *Bridge Inspector's Reference Manual*. United States Department of Transportation, 2012. Print.
- Hartley, Richard, and Andrew Zisserman. *Multiple View Geometry in Computer Vision*. 2nd ed. Cambridge University Press, 2004. *Safari Books Online*. Web. 25 Aug. 2016.
- Autodesk Inventor. San Rafael, CA: Autodesk Inc.
- Jafari, Bahman, Ali Khaloo, and David Lattanzi. "Long-Term Monitoring of Structures through Point Cloud Analysis." *SPIE Smart Structures and Materials+ Nondestructive Evaluation and Health Monitoring*. International Society for Optics and Photonics, 2016. 98052K–98052K. *Google Scholar*. Web. 11 Aug. 2016.
- Jansen, Bart. "Study: 58,000 U.S. Bridges Found to Be 'Structurally Deficient.'" *USA TODAY*. Web. 18 Aug. 2016.

- Kayser, Jack R., and Andrzej S. Nowak. "Capacity Loss due to Corrosion in Steel-Girder Bridges." *Journal of Structural Engineering* 115.6 (1989): 1525–1537. Print.
- Kazhdan, Michael, Matthew Bolitho, and Hugues Hoppe. "Poisson Surface Reconstruction." *Proceedings of the Fourth Eurographics Symposium on Geometry Processing*. Vol. 7. *Google Scholar*. Web. 25 Aug. 2016.
- Lee, H. M., and H. S. Park. "Gage-Free Stress Estimation of a Beam-like Structure Based on Terrestrial Laser Scanning." *Computer-Aided Civil and Infrastructure Engineering* 26.8 (2011): 647–658. *Wiley Online Library*. Web.
- MATLAB R2015a. Natick, MA: MathWorks Inc.
- MeshLab. Italy: ISTI-CNR.
- NACE. "Highways and Bridges." Web. 5 July 2016.
- Richard G. Budynas. *Shigley's Mechanical Engineering Design*. Tenth edition., 2015. Print. McGraw-Hill Series in Mechanical Engineering.
- Sharifi, Yasser, and Reza Rahgozar. "Remaining Moment Capacity of Corroded Steel Beams." *International Journal of Steel Structures* 10.2 165–176. link.springer.com. Web.
- Sugimoto, Ichiro, Yusuke Kobayashi, and Atsushi Ichikawa. "Durability Evaluation Based on Buckling Characteristics of Corroded Steel Deck Girders." *Quarterly Report of RTRI* 47.3 (2006): 150–155. *J-Stage*. Web.
- Torok, Matthew M. "Autonomous Sample Collection Using Image-Based 3D Reconstructions." thesis. Virginia Tech, 2012. vtechworks.lib.vt.edu. Web. 2 Feb. 2016.

van de Lindt, John W., and Theresa M. Ahlborn. "Development of Steel Beam End Deterioration Guidelines." Michigan Department of Transportation (2005): Print.

Zvietcovich, Fernando, Benjamin Castaneda, and Renato Perucchio. "3D Solid Model Updating of Complex Ancient Monumental Structures Based on Local Geometrical Meshes." *Digital Applications in Archaeology and Cultural Heritage* 2.1 (2015): 12–27. *ScienceDirect*. Web.

BIOGRAPHY

Affan Danish Khan graduated from Middle East International High School, Riyadh, Saudi Arabia, in 2009. He received his Bachelor of Engineering in Civil Engineering from NED University of Engineering & Technology, Karachi, Pakistan, in 2013. He will receive his Masters of Science in Structural Engineering from George Mason University, Virginia, in the fall of 2016.